

# Segment to Recognize Robustly – Enhancing Recognition by Image Decomposition

Klara Janouskova    Cristian Gavrus    Jiri Matas  
 Visual Recognition Group, Czech Technical University in Prague  
 {klara.janouskova, gavrucri, matas}@fel.cvut.cz

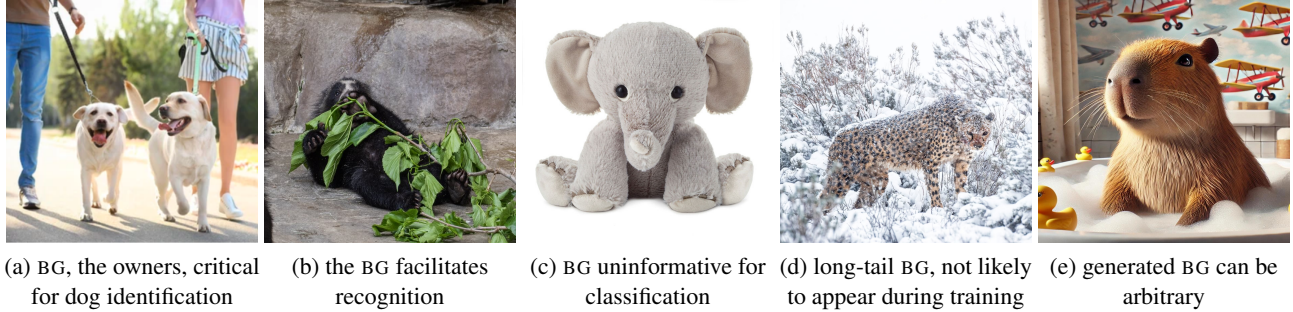


Figure 1. The complementarity of foreground (FG) and background (BG) in recognition. The standard approach, background suppression, makes correct identification in (a) nearly impossible, and difficult in (b); the spectacled bear is the most herbivorous of all bear species. On the other hand, rare backgrounds with possibly huge diversity hurt classification – (d) shows a cheetah after a snowfall in South Africa, not a snow leopard. In generated content (e), any FG can appear on any BG as in ChatGPT 4o’s response to “capybara in a bathroom”.

## Abstract

*In image recognition, both foreground (FG) and background (BG) play an important role; however, standard deep image recognition often leads to unintended over-reliance on the BG, limiting model robustness in real-world deployment settings. Current solutions mainly suppress the BG, sacrificing BG information for improved generalization.*

*We propose “Segment to Recognize Robustly” (S2R<sup>2</sup>), a novel recognition approach which decouples the FG and BG modelling and combines them in a simple, robust and interpretable manner. S2R<sup>2</sup> leverages recent advances in zero-shot segmentation to isolate the FG and the BG before or during recognition. By combining FG and BG, potentially also with standard full image classifier, S2R<sup>2</sup> achieves state-of-the-art results on in-domain data while maintaining robustness to BG shifts. The results confirm that segmentation before recognition is now possible<sup>1</sup>.*

## 1. Introduction

In standard deep image recognition, a neural network models the statistical dependence of the image appearance and

the classes in the training set. It has been highly successful in i.i.d. settings, particularly with moderate to large-scale training data.

As image recognition matured, analyses of its weaknesses [47, 55] revealed that image classifiers are particularly prone to unintended over-reliance on the background (BG)<sup>2</sup>. This seriously impacts model robustness in real-world deployment settings as BG shortcuts [14] perform well on training data but fail to generalize to long-tail BGs, i.e. rarely or never appearing in the training data, and to substantial BG distribution shifts, which are common.

The problem has been predominantly addressed by suppression of BG features. Such methods can be broadly categorized into two classes, the first group emphasizes FG features [2, 6, 8, 57], the second alters the BG distribution [4, 15, 45, 52, 55] through image augmentation and generation techniques.

However, the BG – i.e. the context – is critical for image recognition in many scenarios [1, 11, 35, 39, 49, 50, 60, 61]. As shown in Figures 1 and 2, certain classes or objects are difficult to identify with FG features alone, without the contextual information that BG provides. The nuanced role of BG has been largely overlooked in the recent deep-learning

<sup>1</sup>Website: <https://klarajanouskova.github.io/S2R2/>

<sup>2</sup>FG is defined as the target object pixels; BG as the complement

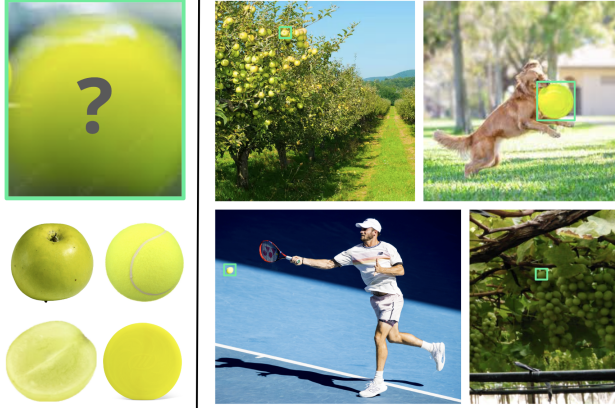


Figure 2. The FG, as in the `cut-outs`, is often ambiguous, especially in low resolution. With the context provided by the BG (right), the uncertainty drops significantly.

oriented literature. In fact, frequently co-occurring FGs and BGs have been referred to as “spuriously” correlated, which misses the point and we challenge such characterization.

This work proposes a novel approach to image recognition. It treats segmentation as an integral part of the recognition process, rather than something more challenging that should only follow classification. The separation of the FG and BG has multiple benefits: The FG and BG modelling is decoupled and thus simplified, avoiding the need to represent all their combinations. The BG modelling can exploit foundational models, since its particular appearance is often irrelevant, unlike its category, like outdoor – indoor, or beach – snow – grass – etc. The FG-BG relationship is only learnt by a lightweight fusion module. In fact, the recognition based on FG-BG segmentation can proceed in parallel with the standard method, see Figure 3, providing robustness when the predictions differ.

We first experimentally confirm that reliance on BG significantly hurts model robustness. We show that a straightforward approach – zero-shot BG removal – is a remarkably strong baseline. It outperforms standard full image modelling on a broad range of benchmarks. We further show that on the Spawrious [28] domain generalization benchmark it outperforms all state-of-the-art approaches that aim at limiting the influence of the BG by modifying their training procedure. These experiments also confirm that BG segmentation as part of recognition, i.e. either class-agnostic or zero-shot, is feasible with modern methods [18, 20, 24, 40, 41, 59].

We proceed to show that by robustly incorporating the BG model in the previous recognition pipeline, the “Segment to Recognize” (S2R<sup>2</sup>) method can leverage the BG and further improve on in-distribution evaluation data, without loss of robustness to BG distribution shifts.

The S2R<sup>2</sup> approach offers additional advantages. The

separation opens up new possibilities for BG modelling, such as leveraging large pretrained models with strong representations of the world, like DINO [36] and CLIP [40], or incorporating diverse data sources, such as tabular metadata related to BG. This allows the BG component to capture context more effectively without extensive additional training, enhancing recognition in highly-varied environments.

To handle cases of segmentation failure, identified through confidence predictions from models like SAM [20], we incorporate a fallback mechanism defaulting to standard recognition which relies on the complete image context, ensuring that classification performance remains stable.

The main contributions of this work are:

1. Introducing S2R<sup>2</sup>, a novel image classification approach that models foreground (FG) and background (BG) independently, enabling robust, context-aware classification. FG and BG representations are combined through a simple, interpretable fusion module.
2. Demonstrating that zero-shot segmentation (without additional training data) can now be integrated into image recognition across a wide range of datasets.
3. Establishing foreground segmentation as a strong baseline for background suppression, achieving state-of-the-art performance across all benchmarks.
4. Showing that our approach achieves state-of-the-art performance on in-domain data while maintaining robustness to background shifts.

## 2. Related work

**Complementary role of FG and BG.** Inspired by human vision, pioneering studies in object detection [11, 35, 50] emphasize the interdependence between FG and BG. These works examine various types of contextual information and demonstrate how contextual cues provide critical insights for recognition, sometimes more so than the object itself. Acharya et al. [1] detect out-of-context objects through context provided by other objects within a scene, modelling co-occurrence through a Graph Neural Network (GNN).

In a recent study, Taesiri et al. [49] dissect the ImageNet dataset [43] into FG, BG, and full-image variants using ground truth bounding boxes. A classifier is trained on each dataset variant, finding that the BG classifier successfully identifies nearly 75% of the images misclassified by the FG classifier. Additionally, they demonstrate that employing zooming as a test-time augmentation markedly improves recognition accuracy.

Closely related to our approach, Zhu et al. [60] advocate for independent modelling of FG and BG with post-training fusion. Unlike our method, which leverages recent advancements in zero-shot segmentation, their approach requires either manual ground truth annotations or computationally intensive edge-based bounding box proposals, averaging 100 predictions per image for each classifier [61]. The exper-

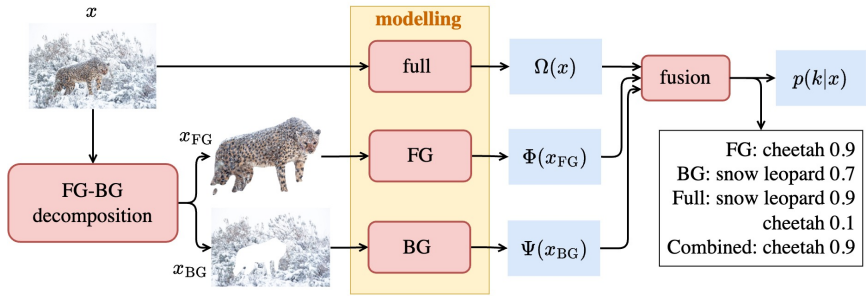


Figure 3. The ‘‘Segment to Recognize Robustly’’ approach – S2R<sup>2</sup> – method proceeds in three stages: (1) decomposition of image  $x$  into FG and BG by zero-shot segmentation, (2) independent modeling of the FG, BG, and the original image (also a fallback option when segmentation fails), and (3) fusion that robustly combines the representations from stage 2 to form predictions  $p(k|x)$ .

iments are limited to a single dataset, a weaker baselines, and employs only a single strategy for combining FG and BG features. In contrast, our work demonstrates the relevance and effectiveness of independent FG-BG modelling even in the era of advanced large-scale models.

Picek et al. [39] investigate the role of FG features and contextual metadata cues, such as time and location, in animal re-identification tasks. Unlike our general approach, their experiments specifically require the presence of ground-truth metadata, focusing on niche applications.

Asgari et al. [3] propose ‘MaskTune’, a method which promotes the learning of a diverse set of features by masking out discriminative features identified by pre-training, without explicitly categorizing these features as FG or BG.

**Background suppression.** The detrimental impact of excessive reliance on BG on classifier robustness to distribution shifts has been well-documented [4, 6, 32, 45, 55]. In response, numerous strategies have been developed to mitigate this over-reliance by suppressing BG during classification. These methods typically involve regularizing classifier training to emphasize FG, either through the use of ground-truth segmentations or attention maps [2, 6, 8, 57]. This enhances FG representation but prevents the classifier from learning BG cues. Moreover, when FG-BG correlations are strong, reliance on attention maps for segmentation proves problematic, as the attention may point to BG [33].

Another group of methods involves training classifiers on images with manipulated or out-of-distribution backgrounds to reduce BG dependency [4, 15, 45, 52, 55]. This technique results in complete disregard of BG information or necessitates selection of FG-BG combinations for effective training, but it is not clear what the optimal distribution should be BG.

Disentangling FG and BG modelling completely eliminates the need for BG suppression.

**Zero-shot segmentation.** Historically, image segmentation has been viewed as a task more complex than image recognition and incorporating segmentation before or during the recognition process was rarely considered feasible. Recent advancements in large vision-language models [24, 40] and class-agnostic, promptable image segmentation

[18, 20, 41, 59] now facilitate zero-shot segmentation. This enables precise localization and effective FG-BG separation across a variety of image classification datasets.

Our methodology leverages these advances and seamlessly integrates robustness against unseen BG while utilizing the inherent information within both FG and BG.

### 3. Method

We propose a novel approach to image recognition that decouples the modelling of the FG and the BG of an image and then combines them by a lightweight interpretable module. The approach consists of three stages: 1. An image decomposition module, 2. FG and BG modelling modules and 3. a fusion module. Figure 3 provides an overview.

#### 3.1. Image decomposition

The goal of this stage is to decompose an image  $x$  into  $x_{FG}$  (pixels representing the target object) and  $x_{BG}$  (the complement of  $x_{FG}$ ). The module comprises two steps:

1. *Segmentation prompt generation* step generates a bounding box or point set localizing the object using a zero-shot object detection model (referred to as  $f_D$ ) such as OWL [30, 31] or GroundingDINO [24]. These models are prompted by a dataset-specific text prompt  $p$ .
2. *FG-BG segmentation* with a model (referred to as  $f_S$ ) like SAM [20] prompted with the output of step 1.

The operation of the image decomposition module can be described as

$$x_{FG}, x_{BG} = f_S(f_D(x, p)) \tag{1}$$

where  $p$  is a dataset-specific text prompt.

**Segmentation prompt generation.** The prompt generation strategy varies with the classification dataset, depending on whether the classes are fine-grained or not and whether the target objects are the dominant objects in an image/if there can be multiple.

*Fine-grained tasks:* The objects in fine-grained recognition belong to a specific meta-class (e.g., recognizing dog breeds or mushroom species). The segmentations in



Figure 4. Different kinds of input to the FG and BG models. FULL is the standard full image, FG<sub>C</sub> is cropped based on the segmentation bounding box, FG<sub>M</sub> is same as FG<sub>C</sub> but with the BG regions masked out, BG<sub>S</sub> is the shape-preserving BG model with FG regions masked out and BG<sub>B</sub> has the area corresponding to the the segmentation bounding box masked out.

such cases is easy – a generic meta-prompt representing all classes (e.g., “dog” or “mushroom”) suffices.

*General case:* In datasets like ImageNet [10], the image may contain an arbitrary number of objects. In such cases, segmentation prior to recognition would require localizing and classifying each object and filtering out those from unknown classes, resulting in an open-set object detection task. A straightforward solution is to map each class to a separate text prompt and consider all options as candidates for segmentation but this does not scale well since there can be thousands of classes in a dataset and many objects in an image, with models like GroundingDINO [24] returning many false-positive detections. We propose a “segmentation during recognition” approach: A standard full-image classifier’s top- $k$  predictions guide the segmentation prompt generation, resulting in up to  $k$  candidate FG regions.

Once the FG and BG regions are identified, different methods (possibly multiple in parallel) can be used to create the images  $x_{FG}$  and  $x_{BG}$ , as illustrated in Figure 4. For FG, two main options are considered: 1. Cropping the image to zoom on the bounding box of FG and 2. Cropping + masking out the BG pixels. For BG, the options of 1. masking out the BG pixels, preserving shape information and 2. masking out the bounding box corresponding to FG are considered. The choice may depend on the dataset and model.

#### Alternative approaches (not explored in this work).

For non-finegrained datasets where a single meta-class does not exist, but the images still contain a single dominant object, the prompt can be something as general as “an object”, a common approach to class-agnostic object detection with vision-language models [29]. This is not the case for any of the datasets explored in this work. Further alternative strategies include co-segmentation methods [12, 25] or generating point/mask prompts using detector attention maps.

### 3.2. Foreground and background modelling

Straightforward standard deep image classification can be employed for both the FG and BG models where a network  $\Phi$  is optimized to output the per-class probability  $p(k|x_{FG}) = \Phi(x_{FG})$  and a network  $\Psi$  to output the per-class probability  $p(k|x_{BG}) = \Psi(x_{BG})$ .

Other options are to use existing pre-trained models and exploit their representation. For instance, large-scale pre-trained models [36, 40] may be particularly suitable for modelling the BG with limited amount of supervision where only high-level abstract concepts such as outdoor-indoor or grass-beach-snow are important, preventing overfitting to incidental particularities of the training images. Another option would be to use different modality such as semantic segmentation or tabular metadata connected to the BG [5, 37].

Thanks to the decoupling of the FG and BG modelling, the FG classifier can not learn BG shortcuts. It also increases interpretability - for instance, if we encounter an object from a well-known class in an unfamiliar environment and  $p(k|x_{BG})$  and  $p(k|x)$  are expected to be low while the probability  $p(k|x_{FG})$  is expected to be much higher.

### 3.3. Fusion modelling

The fusion model is a lightweight module designed to combine the outputs of base classifiers, such as FG and BG. The fusion model’s optimization is independent of the optimization of the fused models, simplifying the fusion task. Rather than learning all  $x_{FG} \times x_{BG}$  combinations, it only learns  $\Phi(x_{FG}) \times \Psi(x_{BG})$ , where  $|\Phi(x_{FG})| \ll |x_{FG}|$  and  $|\Psi(x_{BG})| \ll |x_{BG}|$ . The fusion models are designed with interpretability in mind.

The fusion module can combine various models (e.g., FG+BG or FG+FULL). Although two-model combinations are primarily considered, most methods can be extended to accommodate additional models.

Let two pretrained models be denoted as  $\Phi_1$  and  $\Phi_2$ , which output logit vectors  $\Phi_i(x) = z_i \in \mathbb{R}^C$ . Applying softmax activations yields per-class confidences  $\sigma(z_i)$ . Predictions and their confidences are obtained by  $\hat{y}_i = \operatorname{argmax}_k z_i^{(k)}$  and  $\hat{p}_i = \sigma(z_i)^{(\hat{y}_i)}$ .

Since deep neural networks are known to be poorly calibrated, potentially hindering model comparisons, (multi-)temperature-scaled logits [13, 16] are considered, where applicable. Details are in Appendix B.3.

#### Confidence fusion

1. **Higher confidence:** Selects the prediction with the

highest confidence, setting  $\hat{p} = \max(\hat{p}_1, \hat{p}_2)$ .

2. **Threshold prediction:** Selects  $\hat{y}_1$  if  $\hat{p}_1 > t$ , otherwise  $\max(\hat{p}_1, \hat{p}_2)$ . The parameter  $t$ , where  $t > 0$ , can be optimized to maximize accuracy on the validation set or manually set to limit the influence of  $\Phi_2$  (typically BG).

#### Logit fusion

3. **Average:** Computes  $\hat{y} = \operatorname{argmax}_k(z_1 + z_2)^{(k)}$ .
4. **Weighted average:** Selects  $\hat{y} = \operatorname{argmax}_k(\alpha z_1 + (1 - \alpha)z_2)^{(k)}$ , where  $\alpha \in [0, 1]$  maximizes val. accuracy.

**Learnt logit fusion** The learnt fusion modules introduce more parameters, optimized via cross-entropy on the training set.

5. **Fully-connected:** A shallow FC network  $\Psi$  is trained to predict  $p(k|x) = \Psi(\Phi_1(x), \Phi_2(x))$  from the pretrained models’ logits. This approach tradeoffs more parameters for interpretability and overfitting risk.
6. **Weighted logits:** Generalize the one-parameter weighted average from option 4 by learning per-class weights  $w_1, w_2 \in \mathbb{R}^C$ , combining logits as  $w_1 z_1 + w_2 z_2$ . The overfitting risk is reduced and interpretability retained.

**Multi-object-proposal fusion** For multiple FG segmentation proposals generated based on the top- $k$  predictions of the full classifier, there exists an FG and BG prediction for each proposal. A straightforward approach would be to average all predictions. However, if segmentations represent different regions, averaging might mix predictions for unrelated areas. Instead, only the confidence of the class that generated the proposal is averaged with the proposal confidence for that class.

### 3.4. Feasibility, fallback option

All previously mentioned models rely on the existence of FG and BG, assuming successful zero-shot segmentation. To mitigate issues with failed segmentation, a fallback option is introduced, where FULL prediction is used. Problematic segmentation can be flagged when the detector output is empty or segmentation confidence falls below a threshold.

## 4. Experiments

We evaluate our approach on four image classification datasets, three of which are fine-grained:

- **FungiTastic** [38]: A challenging fine-grained fungi species dataset with complex FG-BG relationships. The BG can be helpful in some cases but may be constant or less informative in others.
- **Hard ImageNet** [33]: A subset of 15 ImageNet [10] classes with strong FG-BG correlations. We also introduce two new test sets for this dataset, **Hard ImageNet - Long Tail (LT)** and **Hard ImageNet - Constant (CT)**, containing unusual or constant BGs to assess model robustness.
- **Spawrious** [28]: A synthetic dog-breed classification dataset introduced for domain generalization. Each class



Figure 5. Extreme BG overfitting on the Fungitastic dataset [38]. Both the FULL (middle column, expected) and BG (right column, surprising) images are correctly classified, with high confidence. The likely reason is the presence of a unique “background” feature, the hand (bottom left) and the existence of a training image (taken in a different year) acquired from a very similar viewpoint (top left). The problem highlights the benefits of the interpretability of S2R<sup>2</sup>: with uncertain FG prediction, one should not pick and eat the mushroom no matter how confident the FULL or BG predictions are. Note: the mushrooms in each row are the same species.

is associated with a specific BG type in the training set, but the BG distribution changes in the test set.

- **Stanford Dogs** [19]: A dataset where the BG plays little role in breed identification.

Additional details concerning the datasets are provided in Appendix A.

### 4.1. Setup

**Evaluation metrics.** Recognition accuracy is reported as the main evaluation metric. For the highly imbalanced FungiTastic, macro-averaged accuracy (mean class-wise accuracy) is used. The result is averaged across five models with different random seeds where available.

**Segmentation.** Segmentation masks are generated as outlined in Section 3.1. For fine-grained datasets, the model is prompted with a meta-class label (“mushroom” for FungiTastic, “full dog” for Stanford Dogs and Spawrious).

For Hard ImageNet, text prompts based on GT labels are used to generate segmentation masks during training. At inference time, we prompt with the top- $k$  predictions of the full image classifier. The detection and segmentation models are OWL [30, 31] and SAM [20]. Masks are generated for 90% of Hard ImageNet images, with negligible rates of mask absence on the other datasets. In Appendix C, results with the GroundingDINO [24] detector are reported.

**Training - base classifiers.** All experiments use ConvNeXt V2-B [26, 54] from Timm [53], pretrained with a fully convolutional masked autoencoder (FCMAE) and fine-tuned on ImageNet-1k, unless indicated otherwise. The classification head is replaced to match the number of classes in each dataset. The input size is  $224 \times 224$  and the batch size

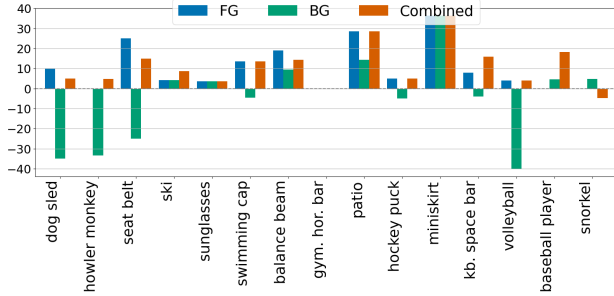


Figure 6. Per-class accuracy % increase or decrease w.r.t. full-image performance on the proposed HardImageNet test set with a significant BG distribution shift. The experiment confirms that  $FG_C$  (cropping image based on segmentation bounding box) is a strong baseline, adding 5.5% in accuracy. The combined approach performs the best, adding 8 % of accuracy. Surprisingly, the BG classifier performs well on about half of the classes, probably due to the information preserved by the mask shape, despite the domain shift.

is 128 for all datasets.

The learning rate is tuned for each dataset, either  $10^{-4}$  or  $5 \times 10^{-5}$ . Horizontal flip (50%) is applied for all datasets, with Random Augment [9] used for FungiTastic as recommended by [38]. The models are optimized by AdamW [27] with the standard cross entropy loss for 20 epochs. Experiments with alternative loss functions (focal, seesaw, balanced CE) yielded no benefits, even for highly unbalanced datasets like FungiTastic. The checkpoints with the best class-averaged  $F_1$  score on the validation set are selected.

We train models for each of the following inputs: FULL images, FG inputs (cropped  $FG_C$  or masked  $FG_M$ ), and BG inputs (with shape  $BG_S$  or bounding box  $BG_B$ ). Each setup is trained with five different seeds unless otherwise stated. Figure 4 illustrates these input variants.

**Evaluation - base classifiers.** For fine-grained datasets, each image has a single mask, and in cases of mask absence, both FG and BG models receive the full image for evaluation consistency. For Hard ImageNet, where multiple segmentation candidates need to be considered, we select the prediction with the highest confidence.

**Fusion models.** Fusion models combine base classifier outputs as per Section 3.3. The standard fusion combines FG and BG (+FULL image classifiers as fallback option), though alternative combinations (e.g., FG + FULL) and different seed variations are also tested.

## 4.2. Results

Detailed tables with evaluation results of the base classifiers (different kinds of FG, BG, and FULL image models), as well as all fusion models on all datasets, are presented in Appendix C. Here, we summarize the main findings and an overview is provided in Table 1.



Figure 7. The unexpected role of shape in BG modelling. When investigating the results on the Hard ImageNet dataset, many examples where full image prediction is **incorrect** but **both** FG and BG (with shape) predictions are **correct**. Possible explanation: the mask provides the BG model with information about the location of the target object and its shape, information not available to unlike the full image model.



Figure 8. Examples where FG model is **correct** and both full image and BG models are **incorrect** on Hard ImageNet - Long Tail.

**Full models.** Standard full-image classification provides a strong baseline across most datasets, with a moderate drop in performance on the HardImageNet Long Tail (by 17%) and CT (by 7%) test sets compared to the original in-distribution test set. A more significant performance drop (from 99.9% to 38.7%) is observed on Spawrious between the validation and test set, where the model overfits to BG due to a substantial BG distribution shift between training and test sets.

**FG models.** The  $FG_C$  variant (cropping based on segmentation bounding box) outperforms full-image models on Fungitastic (by 0.5%), Stanford Dogs (by 1.4%), and Spawrious (by 50.5%). On HardImageNet, it performs best in controlled setups (“cheating setups” where ground truth masks/ground truth labels prompt segmentation) but does not consistently outperform in the general setup without ground truth. Specific improvements include: from 97.31% to 98.03% on the original test set, from 80.88% to 88.23% on LT, and from 89.7% to 95.76% on CT, see Table 3 for more details.  $FG_C$  generally outperforms  $FG_M$  (masked BG pixels) across datasets, except for Spawrious and HardImageNet-CT.

**BG models.** As expected, both BG models perform well on the original Hard ImageNet test set (95 – 96%),

Model	Datasets					
	Fungitastic	HIN-Original	HIN-Long Tail	HIN-Constant	Spawrious	Stanford-Dogs
FG	44.00%±1.15	94.21%±0.77	79.82%±1.83	90.10%±0.76	<b>95.44%±0.56</b>	89.95%±0.45
BG	23.76%±2.08	96.21%±0.43	79.03%±1.93	89.50%±1.76	2.42%±0.66	50.79%±1.56
FG+BG	46.74%±0.84	<b>98.03%±0.13</b>	<b>84.34%±0.66</b>	<b>92.32%±1.76</b>	88.44%±3.39	89.74%±0.41
FG+FULL	<b>48.72%±0.32</b>	—	—	—	84.23%±11.3	<b>91.45%±0.19</b>
FULL	43.50%±0.73	97.31%±0.49	80.88%±1.84	89.7%±1.81	38.73%±8.18	88.52%±0.8
FG×2	48.16%±0.98	—	—	—	96.28%±0.22	91.03%±0.57
Full×2	47.75%±0.54	97.87%±0.19	83.85%±2.19	90.91%±1.43	38.07%±6.07	90.33%±0.03
Oracle FG+BG	49.19%±0.67	98.45%±0.38	87.26%±0.99	95.76%±0.76	95.46%±0.56	91.98%±0.37
Oracle FG+FULL	53.60%±1.01	—	—	—	95.53%±0.57	94.24%±0.28

Table 1. (top) The FG, BG, FULL and fusion models results. FG<sub>C</sub> is used in all experiments except in Spawrious and HIN-Constant. FG×2, FULL×2 - ensembles of two classifiers trained with a different random seed. (bottom) Oracle ensembles providing an upper bound for the fusion models. For Hard ImageNet (HIN) models, FULL prediction is included by default, other combinations with FULL are not meaningful. Recognition accuracy is reported for all the dataset except for the highly imbalanced FungiTastic [38] where the mean class accuracy is reported. Note: the fusion module may differ according to the dataset, for details, see text.

Domain generalization		Ours	
Method	Accuracy	Method	Accuracy
ERM [51]	77.49%	<b>TV</b>	
GroupDRO [44]	80.58%	Full	48.61%
IRM [C]	75.45%	FG <sub>C</sub>	<b>91.68%</b>
CORAL [48]	<b>89.66%</b>	FG <sub>M</sub>	<b>94.39%</b>
CausIRL [7]	89.32%	BG	5.42%
MMD-AAE [22]	78.81%	FG <sub>C</sub> + BG	87.25%
Fish [46]	77.51%	<b>Timm</b>	
VREX [21]	84.69%	Full	87.26%
W2D [17]	81.94%	FG <sub>C</sub>	<b>96.09%</b>
JTT [23]	<b>90.24%</b>	FG <sub>M</sub>	<b>96.01%</b>
Mixup [56]	88.48%	BG	24.96%
Mixup [58]	88.64%	FG <sub>C</sub> + BG	91.65%

Table 2. Spawrious [28] – comparison to domain generalization methods. All methods except for the entries below ‘Timm’, which denotes a model from Pytorch Image Models, correspond to a Resnet50 model from torchvision. The **best** and **second best** results are highlighted. FG<sub>C</sub> denotes cropping based on segmentation bbox, FG<sub>M</sub> also removes the BG pixels from FG<sub>C</sub>. Our results represent a single run while the numbers in the left column represent an average across multiple runs - multi-run results for our methods can be found in Supplementary.

which was designed to contain strong FG-BG correlations. The performance significantly drops on the new Hard ImageNet test sets, with the shape-preserving BG variant showing better robustness. On Spawrious, both BG models perform poorly, while on Stanford Dogs, the shape-preserving BG variant (50.79%) outperforms the non-shape variant but still falls short of FG and full-image models. Interestingly,

HardImageNet Test Set				
	Model	Original	Long Tail	Constant
	FULL	97.31	80.88	89.7
GT masks	FG	98.03	88.23	95.76
	BG	95.33	78.23	66.46
	FG+BG	98.61	90.62	93.94
GT labels	FG	98.00	87.61	94.95
	BG	98.00	79.20	68.69
	FG+BG	98.93	92.48	90.91
w/o GT: Top- <i>k</i> prompting	<b>With fallback option</b>			
	FG	94.21	79.82	90.10
	BG	96.21	79.03	89.50
	FG+BG	98.03	84.34	92.32
	<b>Without fallback option</b>			
	FG	81.07	65.49	66.67
	BG	83.07	65.93	66.67

Table 3. Mean class accuracy on the HardImageNet dataset with different segmentation setups. (top) GT masks, (middle) prompting with GT labels, (middle, bottom) prompting with top-*k* predictions of full image classifier without any ground truth labels or mask, where (bottom) shows the impact of removing the FULL fallback option for cases where segmentation failed.

both BG variants perform well on FungiTastic, with the shape variant roughly doubling performance (23.76%) on this challenging dataset.

**Fusion models.** The performance and suitability of different kinds of fusion model differ for each data set. The

first observation is that temperature scaling almost always helps, no matter which fusion model is used. Overall, the ‘average logits’ fusion model has a fairly stable performance across all datasets. When both FG and BG play an important role in the training set images, such as in the fungitastic datasets, the learnt weighted logits fusion approach usually outperforms the simpler ones. In extreme BG domain shift cases such as in the Spawrious benchmarks, the fusion module may decrease the performance over the FG only classifier while still significantly outperforming the standard full image modelling.

The summary results in Table 1 show that the FG-BG fusion models outperform the base models on all the datasets except for Spawrious (as expected). The combination of FG-FULL also outperforms FG-BG,  $FG \times 2$ ,  $FULL \times 2$  on Fungitastic and Stanford-Dogs, showing it is beneficial to incorporate FULL as more than just a fallback option.

**Comparison to domain generalization methods.** To compare our  $S2R^2$  approach for BG influence suppression to previous domain generalization methods, we provide results of Resnet50 classifiers and compare to the results from Spawrious [28] in Table 2. The experiments are carried out with two Resnet50 models that differ in pretraining. The first variant is the same as the domain generalization methods (torchvision), the second is from Timm. Both FG and fusion models outperform the baselines, the FG model by a large margin. Interestingly, the Timm pretrained Resnet50 model is more robust than the torchvision model, and standard full image modelling with the Timm variant outperforms many of the baseline methods. Again, our method beats the baselines by a large margin.

**Segmentation ablation on Hard Imagent.** In Table 3, a comparison of the fully-automated segmentation to cheating segmentation setups is provided. In the first set of experiments, ground truth segmentation masks from [33] are used to both train and evaluate all the models. In the second set of experiments, ground truth labels are used to create segmentation prompts during both training and evaluation. The last set of experiments is the standard fully-automatic setup which does not use any ground truth.

Surprisingly, the cheating setup with labels sometimes outperforms the ground truth masks. We hypothesize this can be attributed to the poor quality of the GT masks (coarse), compared to the outputs of SAM (clear shape).

**Per-class analysis on Hard ImageNet** where FG, BG and fusion model performance is compared to FULL on new test sets with strong BG shift using GT masks is provided in Figure 6. Examples of **extreme overfitting to BG on Fungitastic** are shown in Figure 5.

Additional experiments with foundational models and tabular metadata are provided in Appendix C.1, C.2.

## 5. Conclusion

This paper introduced “Segment to Recognize Robustly” ( $S2R^2$ ), a novel approach to image recognition.  $S2R^2$  incorporates zero-shot segmentation into the recognition process, enabling the decoupling of FG and BG modelling.

By separating FG and BG features and combining them with a lightweight, interpretable fusion module,  $S2R^2$  enables reaping the benefits of context-aware classification while being robust to long-tail BGs or BG distribution shift.

Our experiments demonstrate that zero-shot BG removal alone is a strong baseline across diverse datasets, consistently outperforming standard full-image models in scenarios both with and without distribution shift. Notably, on the Spawrious [28] domain generalization benchmark, our approach surpassed all domain generalization baselines by a large margin –  $S2R^2$  achieved an accuracy of 94.39 %, while the runner up achieved 90.24 %.

Experiments with combined modelling further show that robustly incorporating BG information to the aforementioned baseline further improves performance on all in-domain datasets with only a small trade-off in terms of robustness to BG distribution shift.

**Limitations.** A primary limitation of this approach is its reliance on vision-language models, which may not generalize as well to niche domains. Additionally, while this work demonstrates the effectiveness of  $S2R^2$ , optimal fusion strategies vary by scenario, no single fusion approach works best across all settings. Finally, we focused on demonstrating the benefits of the proposed approach but it is important to mention our method introduces additional computational complexity by requiring a detector, a segmenter, and multiple classifiers, which increases overhead compared to standard classification pipelines.

**Future work.** This work opens up the space for several directions of future work. First, we envision  $S2R^2$  applied to more general settings by incorporating of class agnostic detectors, removing the reliance on dataset-specific text prompts. Another area consists of exploring other possibilities of FG, BG and fusion modelling. For instance, occlusion is removed in the FG space as part of the BG removal and occlusion data augmentation of the FG input consists of simply masking out portions of the image, without needing to model different textures. Efficiency improvements could leverage strong pretrained representations, such as those in DINOv2 [36], to reduce computational demands. Finally, the proposed approach is applicable to many other computer vision tasks such as object detection and tracking.

## References

- [1] Manoj Acharya, Anirban Roy, Kaushik Koneripalli, Susmit Jha, Christopher Kanan, and Ajay Divakaran. Detecting out-of-context objects using contextual cues. *arXiv preprint arXiv:2202.05930*, 2022. 1, 2
- [2] Ananthu Aniraj, Cassio F Dantas, Dino Ienco, and Diego Marcos. Masking strategies for background bias removal in computer vision models. In *Proceedings of the IEEE/CVF International Conference on Computer Vision*, pages 4397–4405, 2023. 1, 3
- [3] Saeid Asgari, Aliasghar Khani, Fereshte Khani, Ali Gholami, Linh Tran, Ali Mahdavi Amiri, and Ghassan Hamarneh. Masktune: Mitigating spurious correlations by forcing to explore. *Advances in Neural Information Processing Systems*, 35:23284–23296, 2022. 3
- [4] Andrei Barbu, David Mayo, Julian Alverio, William Luo, Christopher Wang, Dan Gutfreund, Josh Tenenbaum, and Boris Katz. Objectnet: A large-scale bias-controlled dataset for pushing the limits of object recognition models. *Advances in neural information processing systems*, 32, 2019. 1, 3
- [5] Thomas Berg, Jiongxin Liu, Seung Woo Lee, Michelle L Alexander, David W Jacobs, and Peter N Belhumeur. Birdsnap: Large-scale fine-grained visual categorization of birds. In *Proceedings of the IEEE conference on computer vision and pattern recognition*, pages 2011–2018, 2014. 4, 15
- [6] Gaurav Bhatt, Deepayan Das, Leonid Sigal, and Vineeth N Balasubramanian. Mitigating the effect of incidental correlations on part-based learning. *Advances in Neural Information Processing Systems*, 36, 2024. 1, 3
- [7] Mathieu Chevalley, Charlotte Bunne, Andreas Krause, and Stefan Bauer. Invariant causal mechanisms through distribution matching. *arXiv preprint arXiv:2206.11646*, 2022. 7
- [8] Po-Yung Chou, Yu-Yung Kao, and Cheng-Hung Lin. Fine-grained visual classification with high-temperature refinement and background suppression. *arXiv preprint arXiv:2303.06442*, 2023. 1, 3
- [9] Ekin D Cubuk, Barret Zoph, Jonathon Shlens, and Quoc V Le. Randaugment: Practical automated data augmentation with a reduced search space. In *Proceedings of the IEEE/CVF conference on computer vision and pattern recognition workshops*, pages 702–703, 2020. 6
- [10] Jia Deng, Wei Dong, Richard Socher, Li-Jia Li, Kai Li, and Li Fei-Fei. Imagenet: A large-scale hierarchical image database. In *2009 IEEE conference on computer vision and pattern recognition*, pages 248–255. Ieee, 2009. 4, 5, 12
- [11] Santosh K Divvala, Derek Hoiem, James H Hays, Alexei A Efros, and Martial Hebert. An empirical study of context in object detection. In *2009 IEEE Conference on computer vision and Pattern Recognition*, pages 1271–1278. IEEE, 2009. 1, 2
- [12] Qi Fan, Deng-Ping Fan, Huazhu Fu, Chi-Keung Tang, Ling Shao, and Yu-Wing Tai. Group collaborative learning for co-salient object detection. In *Proceedings of the IEEE/CVF Conference on Computer Vision and Pattern Recognition*, pages 12288–12298, 2021. 4
- [13] Lior Frenkel and Jacob Goldberger. Network calibration by class-based temperature scaling. In *2021 29th European Signal Processing Conference (EUSIPCO)*, pages 1486–1490. IEEE, 2021. 4, 13
- [14] Robert Geirhos, Jörn-Henrik Jacobsen, Claudio Michaelis, Richard Zemel, Wieland Brendel, Matthias Bethge, and Felix A Wichmann. Shortcut learning in deep neural networks. *Nature Machine Intelligence*, 2(11):665–673, 2020. 1
- [15] Sreyan Ghosh, Chandra Kiran Reddy Evuru, Sonal Kumar, Utkarsh Tyagi, S Sakshi, Sanjoy Chowdhury, and Dinesh Manocha. Aspire: Language-guided data augmentation for improving robustness against spurious correlations. In *Findings of the Association for Computational Linguistics ACL 2024*, pages 386–406, 2024. 1, 3
- [16] Chuan Guo, Geoff Pleiss, Yu Sun, and Kilian Q Weinberger. On calibration of modern neural networks. In *International conference on machine learning*, pages 1321–1330. PMLR, 2017. 4, 13
- [17] Zeyi Huang, Haohan Wang, Dong Huang, Yong Jae Lee, and Eric P Xing. The two dimensions of worst-case training and their integrated effect for out-of-domain generalization. In *Proceedings of the IEEE/CVF Conference on Computer Vision and Pattern Recognition*, pages 9631–9641, 2022. 7
- [18] Lei Ke, Mingqiao Ye, Martin Danelljan, Yu-Wing Tai, Chi-Keung Tang, Fisher Yu, et al. Segment anything in high quality. *Advances in Neural Information Processing Systems*, 36, 2024. 2, 3
- [19] Aditya Khosla, Nityananda Jayadevaprakash, Bangpeng Yao, and Li Fei-Fei. Novel dataset for fine-grained image categorization. In *First Workshop on Fine-Grained Visual Categorization, IEEE Conference on Computer Vision and Pattern Recognition*, Colorado Springs, CO, 2011. 5, 12
- [20] Alexander Kirillov, Eric Mintun, Nikhila Ravi, Hanzi Mao, Chloe Rolland, Laura Gustafson, Tete Xiao, Spencer Whitehead, Alexander C Berg, Wan-Yen Lo, et al. Segment anything. In *Proceedings of the IEEE/CVF International Conference on Computer Vision*, pages 4015–4026, 2023. 2, 3, 5, 12
- [21] David Krueger, Ethan Caballero, Joern-Henrik Jacobsen, Amy Zhang, Jonathan Binas, Dinghuai Zhang, Remi Le Priol, and Aaron Courville. Out-of-distribution generalization via risk extrapolation (rex). In *International conference on machine learning*, pages 5815–5826. PMLR, 2021. 7
- [22] Haoliang Li, Sinno Jialin Pan, Shiqi Wang, and Alex C Kot. Domain generalization with adversarial feature learning. In *Proceedings of the IEEE conference on computer vision and pattern recognition*, pages 5400–5409, 2018. 7
- [23] Evan Z Liu, Behzad Haghgoo, Annie S Chen, Aditi Raghunathan, Pang Wei Koh, Shiori Sagawa, Percy Liang, and Chelsea Finn. Just train twice: Improving group robustness without training group information. In *International Conference on Machine Learning*, pages 6781–6792. PMLR, 2021. 7
- [24] Shilong Liu, Zhaoyang Zeng, Tianhe Ren, Feng Li, Hao Zhang, Jie Yang, Chunyuan Li, Jianwei Yang, Hang Su, Jun Zhu, et al. Grounding dino: Marrying dino with grounded

- pre-training for open-set object detection. *arXiv preprint arXiv:2303.05499*, 2023. 2, 3, 4, 5, 12
- [25] Weide Liu, Chi Zhang, Guosheng Lin, and Fayao Liu. Cr-net: Cross-reference networks for few-shot segmentation. In *Proceedings of the IEEE/CVF conference on computer vision and pattern recognition*, pages 4165–4173, 2020. 4
- [26] Zhuang Liu, Hanzi Mao, Chao-Yuan Wu, Christoph Feichtenhofer, Trevor Darrell, and Saining Xie. A convnet for the 2020s. *Proceedings of the IEEE/CVF Conference on Computer Vision and Pattern Recognition (CVPR)*, 2022. 5
- [27] I Loshchilov. Decoupled weight decay regularization. *arXiv preprint arXiv:1711.05101*, 2017. 6
- [28] Aengus Lynch, Gbètondji J-S Dovonon, Jean Kaddour, and Ricardo Silva. Spawrious: A benchmark for fine control of spurious correlation biases, 2023. 2, 5, 7, 8, 12, 14
- [29] Muhammad Maaz, Hanoona Rasheed, Salman Khan, Fahad Shahbaz Khan, Rao Muhammad Anwer, and Ming-Hsuan Yang. Class-agnostic object detection with multi-modal transformer. In *European conference on computer vision*, pages 512–531. Springer, 2022. 4
- [30] Matthias Minderer, Alexey Gritsenko, Austin Stone, Maxim Neumann, Dirk Weissenborn, Alexey Dosovitskiy, Aravindh Mahendran, Anurag Arnab, Mostafa Dehghani, Zhuoran Shen, et al. Simple open-vocabulary object detection. In *European Conference on Computer Vision*, pages 728–755. Springer, 2022. 3, 5, 13
- [31] Matthias Minderer, Alexey Gritsenko, and Neil Houlsby. Scaling open-vocabulary object detection. *Advances in Neural Information Processing Systems*, 36, 2024. 3, 5, 13
- [32] Mazda Moayeri, Phillip Pope, Yogesh Balaji, and Soheil Feizi. A comprehensive study of image classification model sensitivity to foregrounds, backgrounds, and visual attributes. In *Proceedings of the IEEE/CVF Conference on Computer Vision and Pattern Recognition*, pages 19087–19097, 2022. 3
- [33] Mazda Moayeri, Sahil Singla, and Soheil Feizi. Hard imagenet: Segmentations for objects with strong spurious cues. *Advances in Neural Information Processing Systems*, 35: 10068–10077, 2022. 3, 5, 8, 12
- [34] Mahdi Pakdaman Naeini, Gregory Cooper, and Milos Hauskrecht. Obtaining well calibrated probabilities using bayesian binning. In *Proceedings of the AAAI conference on artificial intelligence*, 2015. 13
- [35] Aude Oliva and Antonio Torralba. The role of context in object recognition. *Trends in cognitive sciences*, 11(12):520–527, 2007. 1, 2
- [36] Maxime Oquab, Timothée Darcet, Théo Moutakanni, Huy Vo, Marc Szafraniec, Vasil Khalidov, Pierre Fernandez, Daniel Haziza, Francisco Massa, Alaaeldin El-Nouby, et al. Dinov2: Learning robust visual features without supervision. *arXiv preprint arXiv:2304.07193*, 2023. 2, 4, 8, 15, 16
- [37] Lukáš Pícek, Milan Šulc, Jiří Matas, Thomas S. Jeppesen, Jacob Heilmann-Clausen, Thomas Læssøe, and Tobias Frøsløv. Danish fungi 2020 - not just another image recognition dataset. In *Proceedings of the IEEE/CVF Winter Conference on Applications of Computer Vision (WACV)*, pages 1525–1535, 2022. 4, 15
- [38] Lukas Pícek, Klara Janouskova, Milan Sulc, and Jiri Matas. Fungitastic: A multi-modal dataset and benchmark for image categorization. *arXiv preprint arXiv:2408.13632*, 2024. 5, 6, 7, 12
- [39] Lukas Pícek, Lukas Neumann, and Jiri Matas. Animal identification with independent foreground and background modeling. *arXiv preprint arXiv:2408.12930*, 2024. 1, 3
- [40] Alec Radford, Jong Wook Kim, Chris Hallacy, Aditya Ramesh, Gabriel Goh, Sandhini Agarwal, Girish Sastry, Amanda Askell, Pamela Mishkin, Jack Clark, et al. Learning transferable visual models from natural language supervision. In *International conference on machine learning*, pages 8748–8763. PMLR, 2021. 2, 3, 4, 15, 16
- [41] Nikhila Ravi, Valentin Gabeur, Yuan-Ting Hu, Ronghang Hu, Chaitanya Ryali, Tengyu Ma, Haitham Khedr, Roman Rädle, Chloe Rolland, Laura Gustafson, et al. Sam 2: Segment anything in images and videos. *arXiv preprint arXiv:2408.00714*, 2024. 2, 3
- [42] Robin Rombach, Andreas Blattmann, Dominik Lorenz, Patrick Esser, and Björn Ommer. High-resolution image synthesis with latent diffusion models. In *Proceedings of the IEEE/CVF conference on computer vision and pattern recognition*, pages 10684–10695, 2022. 12
- [43] Olga Russakovsky, Jia Deng, Hao Su, Jonathan Krause, Sanjeev Satheesh, Sean Ma, Zhiheng Huang, Andrej Karpathy, Aditya Khosla, Michael Bernstein, et al. Imagenet large scale visual recognition challenge. *International journal of computer vision*, 115:211–252, 2015. 2
- [44] Shiori Sagawa, Pang Wei Koh, Tatsunori B Hashimoto, and Percy Liang. Distributionally robust neural networks for group shifts: On the importance of regularization for worst-case generalization. *arXiv preprint arXiv:1911.08731*, 2019. 7
- [45] Rakshith Shetty, Bernt Schiele, and Mario Fritz. Not using the car to see the sidewalk—quantifying and controlling the effects of context in classification and segmentation. In *Proceedings of the IEEE/CVF Conference on Computer Vision and Pattern Recognition*, pages 8218–8226, 2019. 1, 3
- [46] Yuge Shi, Jeffrey Seely, Philip HS Torr, N Siddharth, Awni Hannun, Nicolas Usunier, and Gabriel Synnaeve. Gradient matching for domain generalization. *arXiv preprint arXiv:2104.09937*, 2021. 7
- [47] Sahil Singla and Soheil Feizi. Salient imagenet: How to discover spurious features in deep learning? In *International Conference on Learning Representations*, 2022. 1, 12
- [48] Baochen Sun and Kate Saenko. Deep coral: Correlation alignment for deep domain adaptation. In *Computer Vision—ECCV 2016 Workshops: Amsterdam, The Netherlands, October 8–10 and 15–16, 2016, Proceedings, Part III 14*, pages 443–450. Springer, 2016. 7
- [49] Mohammad Reza Taesiri, Giang Nguyen, Sarra Habchi, Cor-Paul Bezemer, and Anh Nguyen. Imagenet-hard: The hardest images remaining from a study of the power of zoom and spatial biases in image classification. *Advances in Neural Information Processing Systems*, 36, 2024. 1, 2
- [50] Antonio Torralba. Contextual priming for object detection. *International journal of computer vision*, 53:169–191, 2003. 1, 2

- [51] Vladimir Vapnik. Principles of risk minimization for learning theory. *Advances in neural information processing systems*, 4, 1991. 7
- [52] Ke Wang, Harshitha Machiraju, Oh-Hyeon Choung, Michael Herzog, and Pascal Frossard. Clad: A contrastive learning based approach for background debiasing. *arXiv preprint arXiv:2210.02748*, 2022. 1, 3
- [53] Ross Wightman. Pytorch image models. <https://github.com/rwightman/pytorch-image-models>, 2019. 5
- [54] Sanghyun Woo, Shoubhik Debnath, Ronghang Hu, Xinlei Chen, Zhuang Liu, In So Kweon, and Saining Xie. Convnext v2: Co-designing and scaling convnets with masked autoencoders. In *Proceedings of the IEEE/CVF Conference on Computer Vision and Pattern Recognition*, pages 16133–16142, 2023. 5
- [55] Kai Xiao, Logan Engstrom, Andrew Ilyas, and Aleksander Madry. Noise or signal: The role of image backgrounds in object recognition. *arXiv preprint arXiv:2006.09994*, 2020. 1, 3
- [56] Minghao Xu, Jian Zhang, Bingbing Ni, Teng Li, Chengjie Wang, Qi Tian, and Wenjun Zhang. Adversarial domain adaptation with domain mixup. In *Proceedings of the AAAI conference on artificial intelligence*, pages 6502–6509, 2020. 7
- [57] Shengying Yang, Xinqi Yang, Jianfeng Wu, and Boyang Feng. Significant feature suppression and cross-feature fusion networks for fine-grained visual classification. *Scientific Reports*, 14(1):24051, 2024. 1, 3
- [58] Huaxiu Yao, Yu Wang, Sai Li, Linjun Zhang, Weixin Liang, James Zou, and Chelsea Finn. Improving out-of-distribution robustness via selective augmentation. In *International Conference on Machine Learning*, pages 25407–25437. PMLR, 2022. 7
- [59] Xu Zhao, Wenchao Ding, Yongqi An, Yinglong Du, Tao Yu, Min Li, Ming Tang, and Jinqiao Wang. Fast segment anything. *arXiv preprint arXiv:2306.12156*, 2023. 2, 3
- [60] Zhuotun Zhu, Lingxi Xie, and Alan L Yuille. Object recognition with and without objects. *arXiv preprint arXiv:1611.06596*, 2016. 1, 2
- [61] C Lawrence Zitnick and Piotr Dollár. Edge boxes: Locating object proposals from edges. In *Computer Vision—ECCV 2014: 13th European Conference, Zurich, Switzerland, September 6–12, 2014, Proceedings, Part V 13*, pages 391–405. Springer, 2014. 1, 2

## A. Datasets

**FungiTastic** FungiTastic [38] is a challenging fine-grained unbalanced fungi species dataset with complex FG-BG relationships and naturally shifting distribution. In this paper we use the FungiTastic–Mini version of the dataset, where the train set contains observations collected until the end of 2021 (46842 images, 215 species), while the val and test sets consist of observations from 2022 (9450 images, 196 species) and 2023 (10914 images, 193 species), respectively. For rare species, only few samples were collected in the training set, and may be missing in either validation or test set.

The dataset images are accompanied by diverse metadata such as time, GPS location, habitat, substrate, EXIF or toxicity level. The time, substrate and habitat attributes are used to estimate the class priors in some of our experiments.

**Hard ImageNet** The Hard ImageNet dataset [33] is a subset of 15 ImageNet-1K classes [10] with strong FG–BG correlations, as observed in Single et al. [47]. GT segmentation masks are collected using Amazon Mechanical Turk. The objects in this dataset are less centered and the area they cover is below average. Of the  $\approx 19000$  training images we reserve 10% from each class for validation. The test set consists of 750 images.

For the purpose of assessing model robustness, we introduce two new test sets for this data set.

**Hard ImageNet - Long Tail (LT)** contains 226 images with unusual FG-BG combinations, such as “volleyball on snow”.

**Hard ImageNet - Constant (CT)** contains 99 images of essentially constant BGs (commonly co-occurring objects may still appear in the BG, such as snorkel and snorkel mask). See Figure 9 for example images.

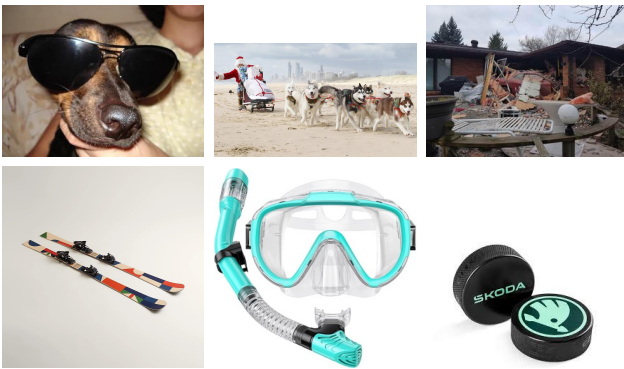


Figure 9. Images from the two new test sets for Hard ImageNet - Long Tail (top) and Constant background (bottom).

**Spawrious** The Spawrious datasets [28] consist of images with strong FG-BG correlations generated using *Stable Dif-*

*fusion v1.4* [42]. We demonstrate our method on the O2O-E Env1 dataset, where each of the 4 dog breed classes is associated with one of the 4 different backgrounds (*Desert, Jungle, Dirt, Snow*) in the training set.

The BGs are permuted in the test set, creating a significant domain shift.

Two variations of the Spawrious dataset are analyzed:

- For the Resnet-50 experiments in the main text and Table 10, where comparisons with the results from the original paper [28] are reported, we follow the process of [28] in which training set FG-BG combinations are set to 97% (e.g. *Bulldogs* appear in *Desert* 97% of the time, and on *Beach* 3% of the time), while test set images for one class always contain the same BG (test *Bulldogs* always appear on *Dirt* BG). See [28][Table 2] for more details.
- For the rest of our Spawrious experiments, including the main paper Table 1 and Table 9, the training correlations are set to 100% as well.

Of the 12672 images in the initial training set, 10% are reserved for validation.

**Stanford Dogs** The Stanford Dogs dataset [19], a curated subset of [10], contains 20580 images of dogs from around the world belonging to 120 species, with  $\approx 150 - 200$  images per class. A large portion of settings are in man-made environments, resulting in larger BG variation compared to other animal datasets. There are no strong FG-BG correlations.

## B. Methods

### B.1. Segmentation

**Fine-grained datasets** For Stanford Dogs and Spawrious datasets, segmentation masks are generated with the text prompt ‘full dog’ while the prompt ‘mushroom’ is used for the FungiTastic.

**Hard ImageNet** The segmentation method is described in the main text, here we provide additional details.

The Segment Anything Model (SAM [20]) provides high-quality masks given points or box prompts. Since the text prompt capability for SAM was not publicly released, a combination of GroundingDINO and SAM was adopted to generate masks for the 3 fine-grained datasets (FungiTastic, Spawrious, Stanford Dogs). Specifically, SAM is prompted with the bounding boxes produced by the open-set object detector Grounding DINO [24] from dataset-specific text prompts, as discussed in the main text.

This works well in cases when it is known a priori that an object matching the text exists in the image. Otherwise, GroundingDINO is prone to false positives. This is the case for Hard ImageNet, where we prompt an image with texts corresponding to multiple labels. Then, false positive FG

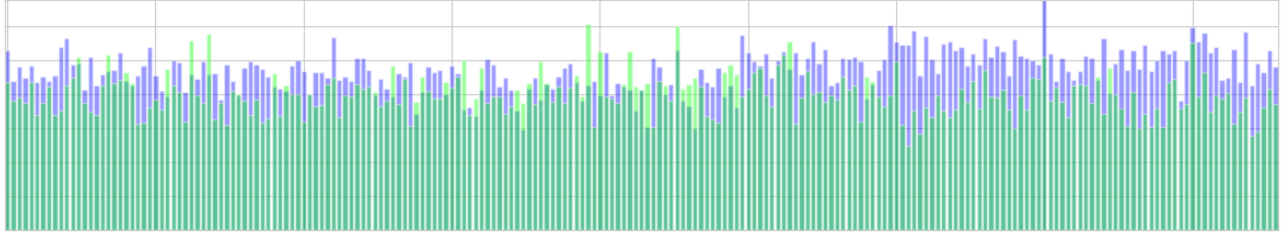


Figure 10. The relative role of **FG** and **BG** for the 215 FungiTastic classes shown by the weights of the learned weighted logits combination model, i.e. Model 9. in Section B.3. The BGs has a higher weight for about 15%

outputs (e.g. a person) correlated to a different class (e.g. sunglasses) may confuse the model. To mitigate this we replace Grounding DINO with the OWLv2 detector [30, 31], at the expense of introducing more false negatives. A comparison of OWLv2 and GroundingDINO in terms of average number of object proposals per image is provided in Figure 11.

## B.2. Input options

We extend the different methods to create the  $x, x_{FG}, x_{BG}$  images introduced in the main text. These are input options for the FULL, FG and BG base classifiers, and represent the rows in Tables 6-8. The different options are:

1. FULL images - the standard approach.
2.  $FG_C$  undistorted: the image is cropped according to the minimal FG segmentation bounding box and padded to preserve the aspect ratio after resizing to a square.
3.  $FG_C$  distorted: Same as  $FG_C$  undistorted but without padding. Since images are automatically resized as inputs for the networks, this version does not preserve the original aspect ration.
4.  $FG_M$  distorted: as before, but the BG pixels are masked out before cropping the image
5.  $FG_M$  undistorted: the BG is fully masked before cropping the square (/padded) bounding box.
6.  $BG_S$ : BG images with shape (the FG are masked, but their shapes remain)
7.  $BG_B$ : BG w/o shape (a minimal segmentation bounding box masks the FG)

## B.3. Combined models

Here we present the fusion models in detail, including the temperature-scaled variants.

We consider two fixed trained models:  $\Phi_1$  and  $\Phi_2$ , which output logit vectors  $\Phi_i(x) = z_i \in \mathbb{R}^C$ , to which softmax activations are applied:  $\sigma(z_i)$ . Predictions are obtained by  $\hat{y}_i = \operatorname{argmax}_k z_i^{(k)}$  and their confidences by  $\hat{p}_i = \max_k \sigma(z_i)^{(k)}$ ,  $i = 1, 2$ .

Since the predictions may be over/under-confident (i.e. the confidences do not reflect the accuracies) and we want

to compare the confidences of different models, we opt for calibrating them using the method of *temperature scaling* [16]. This is done using a single parameter  $T > 0$  for all classes. Given a model  $\Phi$ , the logits and confidences are scaled by

$$z \rightarrow z/T, \sigma(z) \rightarrow \sigma(z/T), \hat{p} \rightarrow \tilde{p} = \max_k \sigma(z/T)^{(k)} \quad (2)$$

Note that the predictions of a fixed model do not change, since the same parameter is applied to all classes. This parameter  $T$  is optimized such that the cross entropy loss is minimized on the *validation* set.

For some datasets it may be desirable to apply different scaling parameters for each class. Such a *class-based temperature scaling* calibration methods was proposed in [13], attempting to minimize the *expected calibration error* (ECE) [34] on the validation set, while not decreasing accuracy, by performing a greedy grid-search. This results in modified logits:

$$z = (z^{(1)}, \dots, z^{(C)}) \rightarrow (z^{(1)}/T_1, \dots, z^{(C)}/T_C) \quad (3)$$

## Confidence fusion

1. (Higher confidence) Between  $\hat{y}_1$  and  $\hat{y}_2$  choose the most confident prediction  $\hat{y}_i$ , i.e. the one with confidence  $\hat{p}_i = \max(\hat{p}_1, \hat{p}_2)$ .
2. (Higher scaled confidence) Again we choose the more confident prediction  $\hat{y}_i$ , but now the confidences are calibrated using temperature scaling (2), originating from  $z_1/T_1, z_2/T_2$ , i.e. choose the one with  $\tilde{p}_i = \max(\tilde{p}_1, \tilde{p}_2)$ .
3. (Higher multi-scaled confidence) Like before, choose the most confident prediction, but now the confidences are calibrated using class-based temperature scaling (3) instead of the single parameter scaling (2).
4. (Threshold prediction) We choose  $\hat{y}_1$  if  $\hat{p}_1 > t$ , otherwise choose the higher confidence prediction. Here  $t > 0$  is a parameter maximizing the new prediction accuracy on the validation set.

### Logit fusion

- (Temperature-scaled logits average) Let  $z_1/T_1, z_2/T_2$  be the scaled logits vectors (2) from the two models and let  $\tilde{z} = \frac{1}{2}(z_1/T_1 + z_2/T_2)$  be their average. The prediction is  $\operatorname{argmax}_k \tilde{z}^{(k)}$  as usual.
- (Temperature-scaled weighted average) As before, but we take a weighted average of the scaled logits,  $\tilde{z} = \alpha z_1/T_1 + (1 - \alpha)z_2/T_2$ , where  $\alpha \in [0, 1]$  maximizes validation set prediction accuracy.
- (Multi-scaled weighted average) As in the previous combination, we take a weighted average, but now we average the class-based scaled logits (3) instead of the single parameter ones (2),

**Learnt fusion** Finally, the predictions learned from the combined logits on the train set are:

- (Concatenate + FC layers) To model the interaction between outputs of  $\Phi_1$  and  $\Phi_2$ , we create new (train, validation and test) datasets by concatenating the logits for each sample  $x$ :

$$\Psi(x) = (\Phi_1(x), \Phi_2(x)) = (z_1, z_2) = (z_1^{(1)}, \dots, z_1^{(C)}, z_2^{(1)}, \dots, z_2^{(C)}) \in \mathbb{R}^{2C} \quad (4)$$

We input (4) into a shallow fully connected network, whose weights are learned from the training set, with cross entropy loss. This can learn more flexible combinations, but it lacks in interpretability and may overfit if the number of classes is large.

- (Weighted logits combination) Here we attempt to generalize the averages from combinations 5-7 by allowing the weights to class-dependent vectors  $w_1, w_2 \in \mathbb{R}^C$ , representing combined logits as  $w_1 z_1 + w_2 z_2 =$

$$(w_1^{(1)} z_1^{(1)} + w_2^{(1)} z_2^{(1)}, \dots, w_1^{(C)} z_1^{(C)} + w_2^{(C)} z_2^{(C)}).$$

We optimize the cross entropy loss instead of the ECE from (3), so gradient descent becomes applicable replacing the grid search. We optimize the weights on the training set instead of the validation set. Compared to the FC model 8, there are much fewer parameters, so there is less risk of overfitting and the network weights are more interpretable (see Fig. 10).

## C. Additional experiments

The setup of the experiments is described in the main text, where only a summary of the results was reported. Exhaustive results of all the base and fusion classifiers for all datasets are reported in Tables 6 - 9.

**Stanford Dogs.** Our experiments show the BG plays little role in breed identification on this dataset, see Table 8.

**Resnet50 experiments on Spawrious.** These additional experiments use a LR of  $10^{-5}$ . As explained in Subsection A, we set the training set FG-BG correlations to 97%

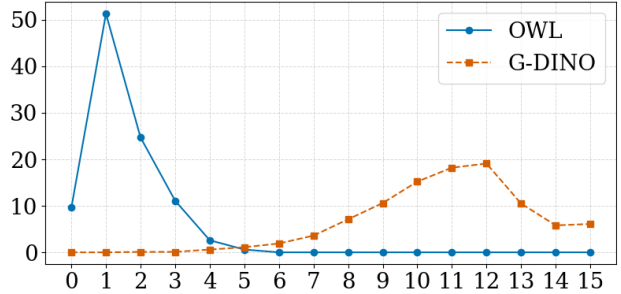


Figure 11. Object detection by OWL+SAM and GroundingDino+SAM on the Hard ImageNet validation set ( $\approx 1900$  images). For each image, the zero-shot detector is prompted for each class, producing  $s \in (0, \dots, 15)$  non-empty segmentation masks. The histogram of the  $s$  values is shown. For example, 51.3% of images get a single OWL+SAM mask. The GroundingDINO results show a higher number of masks. The value of  $k$  is optimized on the validation set.

to compare with the results in [28][Table 2]. The Resnet50 models are initialized with two sets of pretrained weights: from Timm and from torchvision. The results are recorded in Table 10<sup>3</sup>.

**Hard Imagenet with GT masks.** This setting provides an upper bound for the “segmentation during recognition” approach. The results are collected in Table 7. The original test set has strong FG-BG correlations, and therefore BG classifiers score very high (92.16/95.33%) by themselves and FG+BG performs best. On the long-tailed BGs test set, BG underperforms, but the (masked) FG + BG fusion still dominates. On the CT BG test set all fusion models unsurprisingly underperform the (masked) FGs.

	Test	Test LT	Test CT
FG OWL	96.40% $\pm 0.71$	81.06% $\pm 2.06$	90.10% $\pm 1.48$
FG G-DINO	94.27%	78.32%	88.89%
BG OWL	96.45% $\pm 0.46$	79.56% $\pm 1.54$	89.29% $\pm 2.18$
BG G-DINO	95.20%	69.47%	83.84%
Fusion OWL	98.03% $\pm 0.13$	83.98% $\pm 0.71$	91.52% $\pm 1.03$
Fusion G-DINO	97.87%	80.09%	90.91%

Table 4. HardImageNet with automatic FG-BG generation and comparison of OWL vs GroundingDino for object proposal generation. Fusion consists of FULL+FG+BG.

**Hard Imagenet with automatic FG-BG generation** This method was introduced in the text as the “segmentation during recognition” approach: the FULL classifier’s top- $k$

<sup>3</sup>The results in Table 10 are not directly comparable with Table 9 because FG-BG correlations are set differently. Also, the results slightly differ from those in the main text, where a sub-optimal learning rate for the FULL model was used. This does not affect any of the conclusions

predictions guide the segmentation prompt generation. For each sample we input  $k = 3$  possible FG candidates in the FG model (arising from 3 text prompts corresponding to the most probable labels). From the 3 resulting logits vectors we take the entry corresponding to the prompted label, and then we take the maximum one to provide the FG prediction. Similarly for the BG prediction. For the combination we average the logits component of the full image, FG and BG, and again the maximum one provides the final prediction. The results, as well as an OWL-Grounding DINO comparison, are provided in Table 4.

**FungiTastic.** Since this dataset is highly unbalanced, we report the macro-averaged accuracy as the main metric. Due to some rare species, the number of present classes is smaller on the validation and test sets. The *torchmetrics* implementation of the metrics, which we rely on in other experiments, does not account for such a scenario and the metric is implemented manually. Missing classes are removed before averaging the per-class accuracies on the validation and test sets.

The results are summarized in Table 6. The highest mean accuracy is attained by the FG + FULL combination, by a margin of  $\approx 1\%$ . This shows that the BG information (which is part of FULL) is important for this dataset as well.

The learnt weights of the weighted logits fusion model on the FungiTastic dataset are visualized in Figure 10.

### C.1. BG model with FungiTastic metadata

The FungiTastic dataset comes with tabular metadata, some of which are related to the BG. Inspired by the metadata prior model of [5, 37], we study the performance of incorporating various BG-related metadata, namely the habitat, substrate and month, with the FULL and FG<sub>C</sub> models.

Results in Table 5 show that all metadata kinds improve the performance of both models. The habitat helps the most, adding 3.8 % to the 43.5 % baseline of FULL and 4.2 % to the 44 % baseline of FG<sub>C</sub>. For habitat and month, the improvements from metadata fusion are greater for the FG<sub>C</sub> than for the FULL, even though the FG<sub>C</sub> already performs better than FULL. We hypothesize this could be due to the suppression of BG influence in FG<sub>C</sub>, leading to better FG-BG decoupling, which is one of the assumption of the metadata model from [5, 37].

	img	+habitat	+substrate	+month
FULL	43.50	47.26 +3.77	45.42 +1.92	45.19 +1.70
FG <sub>C</sub>	44.00	48.22 +4.22	45.77 +1.77	45.80 +1.81

Table 5. Mean class accuracy of fusion models with BG representation [5, 37] based on tabular metadata (habitat, substrate, month) on the FungiTastic dataset. The increment over image-only performance is also reported. The results are averaged across 5 runs with different random seeds.

### C.2. k-NN on few-shot datasets

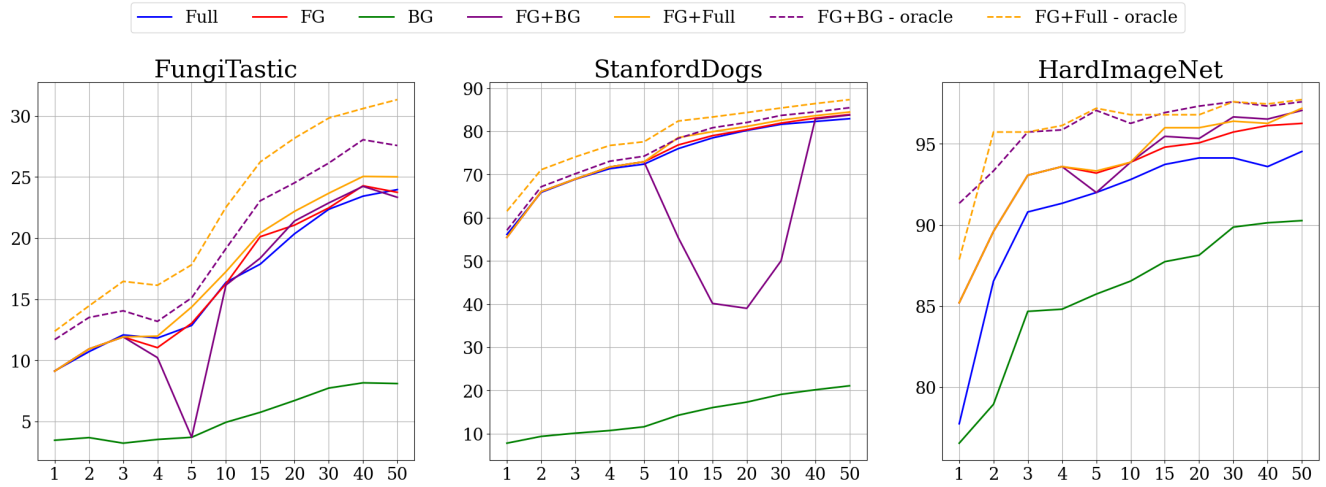
All the previous experiments were conducted in a standard supervised learning setup. Here, we report results of experiments with large-scale self-supervised pretrained models, namely DINOv2 [36] and CLIP [40], in a few-shot learning setup.

The experiments are conducted on the HardImageNet, FungiTastic and StanfordDogs datasets. The  $k$ -shot dataset variants,  $k \in (1, 2, 3, 4, 5, 10, 15, 20, 30, 40, 50)$ , were created by keeping only  $k$  training samples for each class.

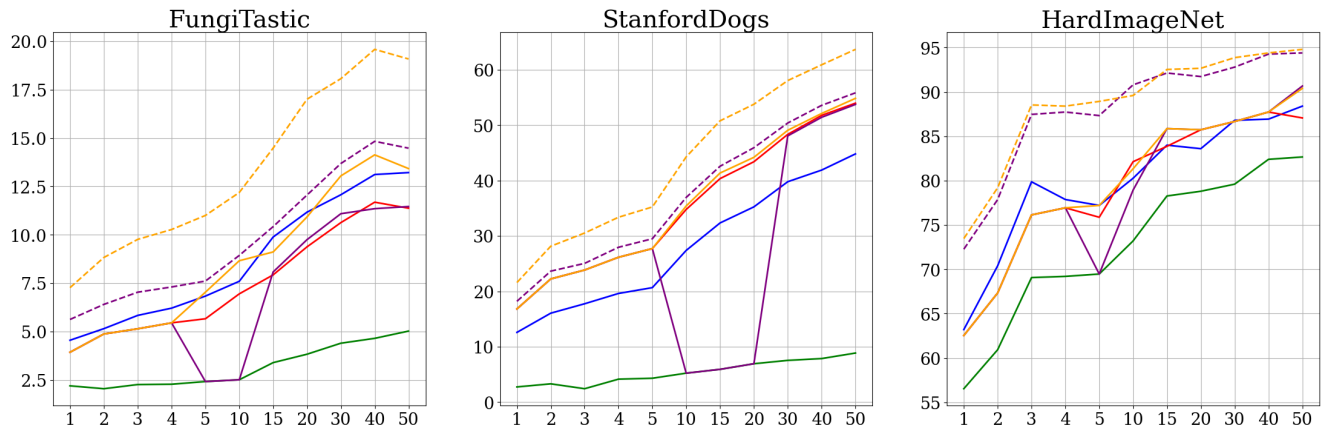
The classifier is the standard k-NN classifier in the embedding space with cosine similarity, where  $k$  is optimized for each dataset on the validation set. The FG<sub>C</sub> (crop, no masking) and BG<sub>S</sub> (preserving shape) variants of FG and BG are reported. Fusion results with FG+BG and FG+FULL where maximum confidence prediction is selected, as well as oracle results where the correct prediction (if it appears among the fused prediction) is selected, are also reported.

The results are shown in Figure 12. We can see that for the DINOv2 model, FG has mostly comparable performance to FULL, except for HardImageNet, where FG is significantly better. Both fusion models help or maintain performance on all datasets, but the BG inclusion significantly hurts performance in some experiments. There is a significant gap between the fusion modules and the upperbound gives by the oracles. The CLIP embeddings significantly underperform the DINOv2 embeddings on all datasets. The FG variant only outperforms FULL on the StanfordDogs dataset. The FULL+FG fusion sometime improves performance, but the inclusion of BG in FG+BG again often hurts.

These results show that the ‘segment to recognize’ method can improve performance even in the few-shot setting with large-scale pretrained models, without any fine-tuning, but there are limitations which should be addressed in future work.



(a) k-NN with DINOv2 embeddings



(b) k-NN with CLIP embeddings

Figure 12. Accuracy of k-NN classifiers – comparison of FG and BG handling methods, the respective line types and colours are listed at the top of the figure. DINOv2 [36] (top) and CLIP [40] (bottom) embeddings on three few-shot dataset – FungiTastic, StanfordDogs and Hard ImageNet. Horizontal axes: the number of training samples in each class (1-50).  $FG_C$  (crop, no masking) and  $BG_S$  (preserving shape) variants of FG and BG are reported. The value of  $k$  is set by optimization on the validations set (separately for each experiment).

Dataset	train acc	train macc	val acc	val macc	test acc	test macc
Full image	93.83% $\pm$ 3.33	86.2% $\pm$ 7.54	68.4% $\pm$ 0.61	45.94% $\pm$ 0.74	66.44% $\pm$ 0.72	43.5% $\pm$ 0.73
FG <sub>C</sub> undistorted	94.23% $\pm$ 3.1	86.84% $\pm$ 7.7	69.34% $\pm$ 0.9	46.88% $\pm$ 0.89	67.54% $\pm$ 0.67	<b>44.0%</b> $\pm$ 1.15
FG <sub>C</sub> distorted	94.7% $\pm$ 3.55	87.99% $\pm$ 8.5	68.93% $\pm$ 0.58	46.22% $\pm$ 0.52	67.3% $\pm$ 0.56	43.65% $\pm$ 0.54
FG <sub>M</sub> distorted	94.38% $\pm$ 2.86	87.99% $\pm$ 6.44	65.23% $\pm$ 0.67	41.88% $\pm$ 0.57	63.69% $\pm$ 0.38	39.48% $\pm$ 0.69
FG <sub>M</sub> undist.	93.15% $\pm$ 1.54	85.09% $\pm$ 4.18	64.79% $\pm$ 0.83	40.77% $\pm$ 0.19	63.35% $\pm$ 1.04	38.95% $\pm$ 0.43
BG <sub>S</sub> : BG w shape	78.88% $\pm$ 6.33	63.0% $\pm$ 8.58	45.27% $\pm$ 2.92	24.73% $\pm$ 2.42	43.1% $\pm$ 2.43	23.76% $\pm$ 2.08
BG <sub>B</sub> : BG w/o shape	74.45% $\pm$ 6.92	62.54% $\pm$ 9.58	21.45% $\pm$ 0.65	10.93% $\pm$ 0.38	19.32% $\pm$ 0.83	10.59% $\pm$ 0.44
Fusion models: FG+BG						
Higher conf	95.19% $\pm$ 3.1	87.79% $\pm$ 8.09	68.47% $\pm$ 0.29	44.19% $\pm$ 0.83	66.83% $\pm$ 0.4	42.37% $\pm$ 0.79
Higher scaled conf	95.13% $\pm$ 3.03	87.62% $\pm$ 7.83	68.52% $\pm$ 0.43	44.31% $\pm$ 0.7	66.78% $\pm$ 0.51	42.19% $\pm$ 0.53
Higher multi-scaled conf	95.23% $\pm$ 2.95	88.36% $\pm$ 7.46	68.9% $\pm$ 0.41	44.74% $\pm$ 0.41	66.93% $\pm$ 0.5	42.65% $\pm$ 0.75
Threshold conf	95.06% $\pm$ 3.11	87.83% $\pm$ 7.98	68.75% $\pm$ 0.48	44.86% $\pm$ 0.79	66.97% $\pm$ 0.51	42.65% $\pm$ 0.67
TempScaled AvgPred	95.67% $\pm$ 2.75	88.79% $\pm$ 7.14	69.28% $\pm$ 0.48	44.9% $\pm$ 0.53	67.62% $\pm$ 0.52	42.93% $\pm$ 0.43
TempScaled WeightedAvg	95.65% $\pm$ 2.88	89.04% $\pm$ 7.48	70.05% $\pm$ 0.51	46.37% $\pm$ 0.4	68.22% $\pm$ 0.58	43.94% $\pm$ 0.68
MultiScaledWeightedAvg	95.75% $\pm$ 2.85	89.7% $\pm$ 7.2	70.3% $\pm$ 0.47	46.85% $\pm$ 0.52	68.35% $\pm$ 0.64	44.26% $\pm$ 0.65
Concatenate + FC layers	98.34% $\pm$ 1.21	96.97% $\pm$ 2.44	69.67% $\pm$ 0.37	48.63% $\pm$ 0.72	68.07% $\pm$ 0.31	45.1% $\pm$ 0.9
WeightedLogitsComb	97.1% $\pm$ 2.03	94.57% $\pm$ 3.79	71.08% $\pm$ 0.45	49.56% $\pm$ 0.63	69.57% $\pm$ 0.41	<b>46.74%</b> $\pm$ 0.84
Fusion: FG + Full image						
WeightedLogitsComb	97.33% $\pm$ 2.29	94.64% $\pm$ 4.36	72.41% $\pm$ 0.35	51.53% $\pm$ 0.62	70.56% $\pm$ 0.36	<b>48.72%</b> $\pm$ 0.32
Fusion: Full image $\times$ 2						
WeightedLogitsComb	98.36% $\pm$ 0.84	96.56% $\pm$ 1.71	71.7% $\pm$ 0.13	50.65% $\pm$ 0.47	69.57% $\pm$ 0.59	47.75% $\pm$ 0.54
Fusion: FG $\times$ 2						
WeightedLogitsComb	97.32% $\pm$ 2.33	94.72% $\pm$ 4.59	72.18% $\pm$ 0.43	51.44% $\pm$ 0.72	70.32% $\pm$ 0.28	47.7% $\pm$ 1.05

Table 6. FungiTastic results

Dataset	train acc	val acc	test-original acc	test-LT acc	test-CT acc
Full image	99.86% $\pm$ 0.1	98.34% $\pm$ 0.06	97.31% $\pm$ 0.49	80.88% $\pm$ 1.84	89.7% $\pm$ 1.81
FG <sub>C</sub> undistorted	99.85% $\pm$ 0.22	98.98% $\pm$ 0.1	<b>98.03%</b> $\pm$ 0.48	<b>88.23%</b> $\pm$ 1.11	90.51% $\pm$ 2.09
FG <sub>C</sub> distorted	99.92% $\pm$ 0.1	98.59% $\pm$ 0.13	97.63% $\pm$ 0.5	87.79% $\pm$ 0.97	90.71% $\pm$ 1.81
FG <sub>M</sub> distorted	97.7% $\pm$ 0.11	95.9% $\pm$ 0.03	95.73% $\pm$ 0.34	85.13% $\pm$ 0.86	94.95% $\pm$ 2.02
FG <sub>M</sub> undist.	97.56% $\pm$ 0.16	95.5% $\pm$ 0.11	95.52% $\pm$ 0.22	84.42% $\pm$ 1.96	<b>95.76%</b> $\pm$ 1.94
BG <sub>S</sub>	99.86% $\pm$ 0.11	97.67% $\pm$ 0.15	95.33% $\pm$ 0.53	78.23% $\pm$ 0.66	66.46% $\pm$ 4.19
BG <sub>B</sub>	99.43% $\pm$ 0.32	93.77% $\pm$ 0.15	92.16% $\pm$ 0.26	58.67% $\pm$ 1.39	27.68% $\pm$ 0.9
Fusion: FG <sub>C</sub> +BG					
Higher conf: FG vs BG	99.98% $\pm$ 0.02	99.06% $\pm$ 0.19	98.43% $\pm$ 0.27	87.35% $\pm$ 1.31	85.25% $\pm$ 2.09
Higher scaled conf	99.96% $\pm$ 0.06	99.18% $\pm$ 0.07	98.59% $\pm$ 0.18	88.14% $\pm$ 1.1	87.27% $\pm$ 2.21
Higher multi-scaled conf	99.96% $\pm$ 0.07	99.18% $\pm$ 0.1	98.59% $\pm$ 0.18	87.7% $\pm$ 0.96	87.68% $\pm$ 2.19
Threshold conf	99.94% $\pm$ 0.08	99.22% $\pm$ 0.07	98.51% $\pm$ 0.17	88.32% $\pm$ 1.55	88.69% $\pm$ 2.3
TempScaled AvgPred	99.96% $\pm$ 0.06	99.22% $\pm$ 0.06	<b>98.61%</b> $\pm$ 0.15	88.32% $\pm$ 0.86	87.47% $\pm$ 1.97
TempScaled WeightedAvg	99.94% $\pm$ 0.08	99.23% $\pm$ 0.06	98.43% $\pm$ 0.17	88.85% $\pm$ 1.58	89.49% $\pm$ 1.69
MultiScaledWeightedAvg	99.95% $\pm$ 0.08	99.2% $\pm$ 0.07	98.48% $\pm$ 0.18	88.67% $\pm$ 1.64	88.69% $\pm$ 1.81
Concatenate + FC layers	99.98% $\pm$ 0.02	99.13% $\pm$ 0.14	98.35% $\pm$ 0.38	87.61% $\pm$ 1.21	85.25% $\pm$ 3.16
WeightedLogitsComb	99.99% $\pm$ 0.02	99.24% $\pm$ 0.14	98.59% $\pm$ 0.18	87.96% $\pm$ 1.01	86.06% $\pm$ 1.66
Fusion: FG (with BG masking) +BG					
Threshold conf	99.96% $\pm$ 0.03	98.94% $\pm$ 0.09	98.08% $\pm$ 0.36	90.09% $\pm$ 1.92	<b>93.94%</b> $\pm$ 1.89
TempScaled AvgPred	99.97% $\pm$ 0.02	98.96% $\pm$ 0.11	98.24% $\pm$ 0.3	<b>90.8%</b> $\pm$ 1.91	93.33% $\pm$ 1.69
Fusion: Full image $\times$ 2					
Higher multi-scaled conf	99.94% $\pm$ 0.05	98.4% $\pm$ 0.11	97.87% $\pm$ 0.19	83.19% $\pm$ 1.88	89.9% $\pm$ 0.0

Table 7. HardImageNet results using GT masks (‘cheating’ setup)

Dataset	train acc	val acc	test acc
Full image	96.72% $\pm$ 2.14	89.0% $\pm$ 0.22	88.52% $\pm$ 0.8
FG <sub>C</sub> undistorted	99.17% $\pm$ 0.73	90.23% $\pm$ 0.6	<b>89.95%</b> $\pm$ 0.45
FG <sub>C</sub> distorted	98.82% $\pm$ 0.69	89.9% $\pm$ 0.44	89.6% $\pm$ 0.37
FG <sub>M</sub> distorted	97.56% $\pm$ 2.13	88.44% $\pm$ 0.54	88.13% $\pm$ 0.37
FG <sub>M</sub> undist.	96.25% $\pm$ 2.62	80.71% $\pm$ 16.49	80.28% $\pm$ 16.86
BG <sub>S</sub> : BG w shape	96.75% $\pm$ 2.52	51.46% $\pm$ 1.48	50.79% $\pm$ 1.56
BG <sub>B</sub> :: BG w/o shape	94.8% $\pm$ 5.57	8.3% $\pm$ 2.7	8.1% $\pm$ 2.33
Fusion models FG+BG			
Higher conf: FG vs BG	99.49% $\pm$ 0.4	87.79% $\pm$ 1.79	87.53% $\pm$ 2.09
Higher scaled conf	99.33% $\pm$ 0.38	89.34% $\pm$ 0.35	89.17% $\pm$ 0.44
Higher multi-scaled conf	99.32% $\pm$ 0.38	89.54% $\pm$ 0.45	89.16% $\pm$ 0.46
Threshold conf	99.01% $\pm$ 0.57	89.7% $\pm$ 0.39	89.5% $\pm$ 0.36
TempScaled AvgPred	99.41% $\pm$ 0.36	89.42% $\pm$ 0.45	89.24% $\pm$ 0.44
TempScaled WeightedAvg	98.98% $\pm$ 0.54	90.1% $\pm$ 0.37	<b>89.74%</b> $\pm$ 0.41
MultiScaledWeightedAvg	99.13% $\pm$ 0.42	90.21% $\pm$ 0.39	89.69% $\pm$ 0.44
Concatenate + FC layers	99.83% $\pm$ 0.1	84.81% $\pm$ 4.65	84.84% $\pm$ 4.73
WeightedLogitsComb	99.59% $\pm$ 0.33	88.62% $\pm$ 1.17	88.52% $\pm$ 1.17
Fusion FG + Full image			
Concatenate + FC layers	99.64% $\pm$ 0.45	91.44% $\pm$ 0.23	<b>91.45%</b> $\pm$ 0.19

Table 8. Stanford dogs.

Dataset	train accuracy	val accuracy	test accuracy
Full image	100.0% $\pm$ 0.0	99.98% $\pm$ 0.02	38.73% $\pm$ 8.18
FG <sub>C</sub> undistorted	99.99% $\pm$ 0.01	99.93% $\pm$ 0.03	85.03% $\pm$ 7.27
FG <sub>C</sub> distorted	100.0% $\pm$ 0.01	99.93% $\pm$ 0.04	89.25% $\pm$ 4.28
FG <sub>M</sub> distorted	99.98% $\pm$ 0.03	99.69% $\pm$ 0.05	95.25% $\pm$ 1.27
FG <sub>M</sub> undist.	99.97% $\pm$ 0.02	99.75% $\pm$ 0.07	<b>95.44%</b> $\pm$ 0.56
BG <sub>S</sub>	100.0% $\pm$ 0.0	99.86% $\pm$ 0.04	2.42% $\pm$ 0.66
BG <sub>B</sub>	99.96% $\pm$ 0.03	99.22% $\pm$ 0.09	0.17% $\pm$ 0.05
Fusion models FG+BG			
Higher conf: FG vs BG	100.0% $\pm$ 0.0	100.0% $\pm$ 0.0	42.05% $\pm$ 17.32
Higher scaled conf	100.0% $\pm$ 0.0	100.0% $\pm$ 0.0	34.8% $\pm$ 20.38
Higher multi-scaled conf	100.0% $\pm$ 0.0	100.0% $\pm$ 0.0	42.15% $\pm$ 22.82
Threshold confidence	100.0% $\pm$ 0.0	100.0% $\pm$ 0.0	<b>88.44%</b> $\pm$ 3.39
TempScaled AvgPred	100.0% $\pm$ 0.0	100.0% $\pm$ 0.0	36.84% $\pm$ 20.27
TempScaled WeightedAvg	100.0% $\pm$ 0.0	99.99% $\pm$ 0.02	39.95% $\pm$ 46.73
MultiScaledWeightedAvg	100.0% $\pm$ 0.0	99.99% $\pm$ 0.02	40.3% $\pm$ 46.54
Concatenate + FC layers	100.0% $\pm$ 0.0	99.98% $\pm$ 0.02	39.22% $\pm$ 30.51
WeightedLogitsComb	100.0% $\pm$ 0.0	100.0% $\pm$ 0.0	49.43% $\pm$ 14.03

Table 9. Result of ConvNeXt models on the Spawrious dataset.

Dataset	Train acc	Val acc	Test acc
Timm Resnet50			
Full image	99.76% $\pm$ 0.06	99.3% $\pm$ 0.19	87.38% $\pm$ 0.71
FG <sub>C</sub> undistorted	99.46% $\pm$ 0.05	99.12% $\pm$ 0.1	95.02% $\pm$ 1.04
FG <sub>C</sub> distorted	99.06% $\pm$ 0.08	98.34% $\pm$ 0.22	94.26% $\pm$ 0.95
FG <sub>M</sub> distorted	98.81% $\pm$ 0.03	98.36% $\pm$ 0.11	94.83% $\pm$ 0.29
FG <sub>M</sub> undist.	99.06% $\pm$ 0.19	98.69% $\pm$ 0.17	95.42% $\pm$ 0.52
BG <sub>S</sub>	98.66% $\pm$ 0.12	97.54% $\pm$ 0.12	24.26% $\pm$ 4.39
BG <sub>B</sub>	95.67% $\pm$ 0.13	94.89% $\pm$ 0.27	0.72% $\pm$ 0.14
FG+BG fusion: Threshold conf	99.79% $\pm$ 0.05	99.55% $\pm$ 0.04	91.37% $\pm$ 0.8
Torchvision Resnet50			
Full image	100.0% $\pm$ 0.0	99.85% $\pm$ 0.04	71.35% $\pm$ 3.72
FG <sub>C</sub> undistorted	100.0% $\pm$ 0.0	99.83% $\pm$ 0.05	95.0% $\pm$ 0.63
FG <sub>C</sub> distorted	99.99% $\pm$ 0.01	99.61% $\pm$ 0.08	94.97% $\pm$ 0.44
FG <sub>M</sub> distorted	100.0% $\pm$ 0.0	99.42% $\pm$ 0.08	95.22% $\pm$ 0.12
FG <sub>M</sub> undist.	100.0% $\pm$ 0.0	99.58% $\pm$ 0.05	95.59% $\pm$ 0.25
BG <sub>S</sub>	100.0% $\pm$ 0.0	99.21% $\pm$ 0.16	8.9% $\pm$ 1.38
BG <sub>B</sub>	99.76% $\pm$ 0.3	96.94% $\pm$ 0.08	0.36% $\pm$ 0.03
FG+BG fusion: Threshold conf	100.0% $\pm$ 0.0	99.91% $\pm$ 0.06	86.78% $\pm$ 3.95

Table 10. Spawrious. Resnet50 models with two different initializations (timm and torchvision).